Int. J. Electrochem. Sci., 7 **(2012)** 1319 - 1331

International Journal of
ELECTROCHEMICAL
SCIENCE
www.electrochemsci.org

In Situ Synthesis of $CoSb_3$-Nanocrystals/Graphene Hybrid Via One-Pot Solvothermal Route and its Electrochemical Li-Storage Properties

Jian Xie, Yun-Xiao Zheng, Shuang-Yu Liu, Wen-Tao Song, Yun-Guang Zhu, Gao-Shao Cao, Tie-Jun Zhu and Xin-Bing Zhao[*]

Department of Materials Science and Engineering, Zhejiang University, Hangzhou 310027, China
[*]E-mail: zhaoxb@zju.edu.cn

Received: 27 December 2011 / *Accepted:* 17 January 2012 / *Published:* 1 February 2012

A $CoSb_3$-nanocrystals/graphene nanocomposite was synthesized by a facile in situ one-pot solvothermal route. $CoSb_3$ nanocrystals (around 10 nm) with a narrow size distribution were uniformly dispersed and supported by the graphene sheets, forming a unique hybrid nanostructure. The electrochemical Li-storage performance of the nanocomposite was investigated as a potential application in Li-ion batteries. The nanocomposite exhibits an obviously improved electrochemical performance compared to bare $CoSb_3$. The enhancement of the electrochemical performance could be attributed to the introduction of the graphene that not only constructs a two-dimensional conductive network but also disperses and confines the $CoSb_3$ nanoparticles. The electronic conductivity and ac impedance were measured to understand the underlying mechanism for the enhanced electrochemical performance.

Keywords: $CoSb_3$, graphene, nanocomposite, Li-storage properties, anode

1. INTRODUCTION

In recent years, a renewed interest has been paid to the metal or alloy anodes for Li-ion batteries due to their high specific capacities. Among them, Sb-based alloys [1−10] have been received special attention because of their flat potential plateaus and large Li-storage capacities with the formation of a Li_3Sb composition. $CoSb_3$ is a typical Sb-based alloy, composed of Li-active Sb and Li-inert Co. The electrochemical Li-storage properties of this material were first reported by Tirado et al. [1]. It was found that $CoSb_3$ showed a better cycling stability than pure Sb due to the presence of the inert Co. This material can yield a theoretical gravimetric capacity of 568 mAh g^{-1} when Li_3Sb is formed, greatly higher than that of graphite (372 mAh g^{-1}). This material, however, undergoes a rapid

capacity fading because of the large volume changes upon Li-absorption/extraction. An effective method to buffer the volume changes is to disperse metal or alloy particles on a matrix. As reported by Dimov et al. [11], the electrochemical performance of Si anode could be greatly improved by using graphite as the buffering matrix. For $CoSb_3$ alloy, some carbon-based materials, such as carbon nanotubes [12], amorphous carbon [13], graphite [14] and mesocarbon microbeads (MCMB) [15] have been considered as the ideal matrix materials because they not only enhance the electronic conductivity but also contribute to the overall capacity, in addition to the dispersing and buffering effects.

Graphene, a flat monolayer of sp^2-bonded carbon atoms, has attracted a considerable interest since first discovered by Novoselov group in 2004 [16]. The combined merits of high electronic conductivity [17], large specific surface area [18] and high mechanical strength [19] make it a promising matrix to support nanosized anodes for Li-ion batteries. Recent investigations on some anodes, such as Sn [20, 21], Si [22, 23], Co_3O_4 [24−29], CoO [29, 30], Fe_3O_4 [31−36], Fe_2O_3 [30, 37, 38], CuO [39, 40], Mn_3O_4 [41], TiO_2 [42, 43], and SnO_2 [44−48] have shown that the electrochemical performance of these materials can be remarkably enhanced by loading them onto the graphene sheets. The flexible graphene acts not only as a buffer to accommodate the large volume changes during Li-absorption/extraction processes but also as a separator to hinder the aggregation of the nanoparticles upon repeated cycling.

To date, the preparation and electrochemical studies on the alloy/graphene nanocomposite anodes, however, were rarely reported [49, 50]. Herein, we report the preparation of $CoSb_3$/graphene nanocomposite by a facile in situ one-pot solvothermal route. The new form of carbon materials, graphene, was selected as the matrix material due to its special advantages as mentioned above. In addition, the composite was prepared by an in situ route, namely, $CoSb_3$ and graphene form simultaneously during the solvothermal process. The electrochemical tests showed that the $CoSb_3$/graphene nanocomposite exhibits an improved electrochemical performance compared with bare $CoSb_3$, indicating a potential application as anode for Li-ion batteries.

2. EEPERIMENTAL SECTION

2.1 Synthesis of graphite oxide

Graphite oxide was synthesized by the modified Hummer's method [51]. In a typical procedure, 5 g of natural graphite powder, 2.5 g of P_2O_5 and 2.5 $K_2S_2O_8$ were added into 39 mL of 98 wt.% H_2SO_4 and magnetically stirred at 80 ºC for 6 h. After cooling down to room temperature, the resulting product was washed with deionized water sufficiently and dried under vacuum at 30 ºC for 8 h to obtain pre-oxidized graphite. The pre-oxidized graphite (2 g), $NaNO_3$ (1 g), and $KMnO_4$ (6 g) were added slowly to 46 mL of 98 wt.% H_2SO_4 and stirred in ice-bath for 1 h. The temperature was then increased to 35 ºC and maintained for 2 h under stirring followed by adding 92 mL of warm water (70 ºC). Then, 200 mL of warm water (70 ºC), 10 mL of 30 wt.% H_2O_2 and 24 mL of 5 wt.% HCl were

successively added to the above solution. Yellow-brown graphite oxide was obtained after centrifugation, washing repeatedly with deionized water, and vacuum-drying at 30 ºC overnight.

2.2 Synthesis of $CoSb_3$/graphene nanocomposite

For the preparation of the $CoSb_3$/graphene nanocomposite, graphite oxide (21 mg) was ultrasonically dispersed in 60 mL of absolute ethanol for 3 h to get exfoliated graphene oxide using an ultrasonic bath (KQ5200B, Kunsan Ultrasonic Instrument Co., Ltd., China). Subsequently, 0.5 mmol of $CoCl_2 \cdot 6H_2O$ and 1 mmol of $SbCl_3$ were added to the above solution. After sonication for another 0.5 h, 20 mL of 0.7 M $NaBH_4$ ethanol solution was slowly added to the mixed solution to reduce Co^{2+} and Sb^{3+} to metallic Co and Sb. The mixture was transferred to a Teflon-lined stainless steel autoclave (100 mL) and heated at 180 ºC for 24 h in an electric oven. During the solvothermal process, Co and Sb were converted into $CoSb_3$ [52] and graphite oxide was reduced to graphene by $NaBH_4$ [53]. The resultant product was separated by centrifugation, washed with deionized water and dried at 30 ºC under vacuum overnight. The formation mechanism of $CoSb_3$ alloy is similar to that of CoSn in polyol reported by González et al. [54]. The Bare $CoSb_3$ was prepared using the similar process for comparison without adding graphite oxide. Bare graphene was prepared by a similar procedure. A simple $CoSb_3$/graphene mixture was also prepared by grinding bare $CoSb_3$ and graphene with a weight ratio of 94.2:5.8, based on the composition analysis of the in situ prepared $CoSb_3$/graphene composite.

2.3 Materials Characterizations

The crystalline structures of the products were characterized by X-ray diffraction (XRD) on a Rigaku D/Max-2550pc powder diffractometer equipped with Cu K_α radiation (λ = 1.54 Å). The morphologies of the products were observed by field emission scanning electron microscopy (SEM) on a FEI-sirion microscope, transmission electron microscopy (TEM) and high-resolution TEM (HRTEM) on a JEM 2100F microscope. Raman spectra were recorded on a Jobin-Yvon Labor Raman HR-800 Raman system by exciting a 514.5 nm Ar^+ laser. X-ray photoelectron spectroscopy (XPS) measurements were performed on a KRATOS AXIS ULTRA-DLD spectrometer with a monochromatic Al K_α radiation (hv = 1486.6 eV). The carbon content analysis was conducted on a Flash EA 1112 tester. The electronic conductivity measurements were conducted by a 4-probe method at room temperature. The pellet samples for the measurements were prepared by sintering the solvothermal products at 550 °C for 30 min under 40 MPa in vacuum.

2.4 Electrochemical measurements

The electrochemical properties of the active materials ($CoSb_3$/graphene, bare $CoSb_3$ and graphene) were evaluated with coin cells (CR 2025). The slurry was made by dispersing active material, acetylene black and polyvinylidene fluoride (PVDF) (75:15:10 in weight) in N-methyl pyrrolidone (NMP) under magnetic stirring. The working electrodes were made by coating the slurry

onto Ni foam. After drying at 100 °C under vacuum for 8 h, the working electrodes were assembled into half cells in an argon-filled glove box using metallic Li foil as the counter electrode, 1 M $LiPF_6$ in ethylene carbonate (EC)-dimethyl carbonate (DMC) (1:1 in volume) as the electrolyte, and polypropylene micro-porous film (Celgard 2300) as the separator. The cells were galvanostatically cycled on a LHS-B-5V5mA8D battery tester in the voltage range of 0.05−1.5 V (vs. Li/Li^+) at various current densities. For the $CoSb_3$/graphene composite, the specific capacity (mAh g^{-1}) values are referred to the masses of both $CoSb_3$ and graphene. Cyclic voltammetry (CV) measurements were performed on an Arbin BT2000 system at 0.05−2 V (vs. Li/Li^+) at 0.1 mV s^{-1}. Electrochemical impedance spectroscopy (EIS) measurements were carried out on a CHI660C electrochemical workstation using two-electrode coin cells. The impedance spectra were recorded by applying an ac signal of 5 mV amplitude over the frequency range from 10^5 Hz to 10 mHz at de-lithiation state. All of the electrochemical measurements were conducted at room temperature.

3. RESULTS and DISCUSSION

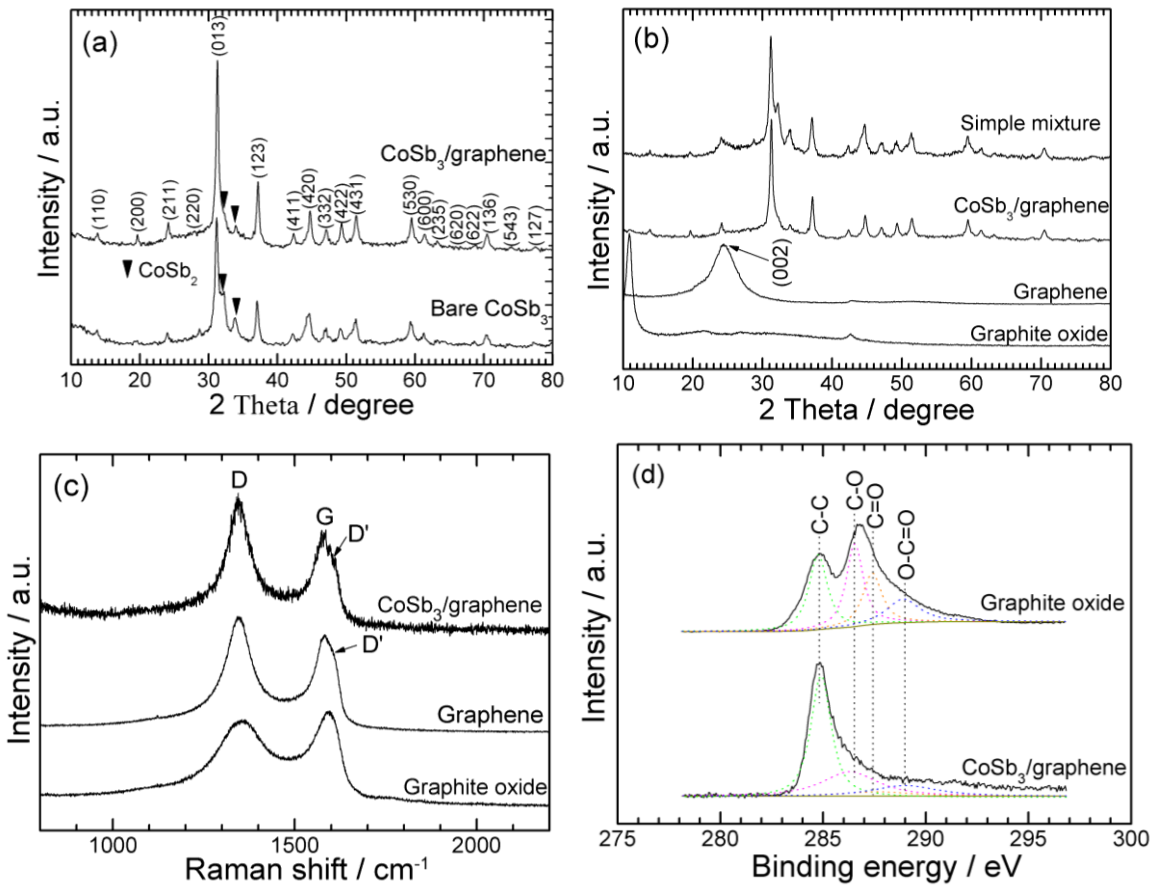

Figure 1. (a) XRD patterns of bare $CoSb_3$ and $CoSb_3$/graphene, (b) XRD patterns of graphite oxide, graphene, $CoSb_3$/graphene and a simple mixture of bare $CoSb_3$ and graphene, (c) Raman spectra of graphite oxide, graphene and $CoSb_3$/graphene, and (d) C1s XPS of graphite oxide.

Fig. 1(a) shows the XRD patterns of the $CoSb_3$/graphene composite and bare $CoSb_3$. The dominant diffraction peaks of both samples can be indexed to skutterudite-type $CoSb_3$ (space group *Im*3, JCPDS No. 76-0470). Minor $CoSb_2$ diffraction peaks are also observed for both samples. The broad diffraction peaks suggest that the particle size of $CoSb_3$ is rather small. The content of graphene is estimated to be 5.8 wt. % by carbon content analysis. The diffraction peak of graphene (002 plane), however, is absent for the composite. Similar phenomenon was also observed in the M/graphene composites (M = Pt, Au, Pd) [55, 56]. In contrast, the simple $CoSb_3$/graphene mixture (5.8 wt. % graphene) prepared by grinding bare $CoSb_3$ and graphene shows a broad diffraction peak, which is superimposed from the (211) peak of $CoSb_3$ and the (002) peak of graphene as seen Fig. 1(b). We suggest that the restacking of the reduced graphene oxide sheets is refrained by homogeneously loading of $CoSb_3$ particles in between the graphene sheets. Nevertheless, the above supposition can only be partly supported by the XRD due to the low graphene content and the superimposition of the peaks. It will be further confirmed by SEM and TEM observations as discussed in the next sections. The interaction between the positively charged metal ions (Co^{2+} and Sb^{3+}) and the negatively charged graphene oxide sheets with different oxygen-containing groups [57] during the early reaction stage plays an important role in the uniform attachment of the $CoSb_3$ particles on graphene.

Fig. 1(c) shows the Raman spectra of $CoSb_3$/graphene, graphene and graphite oxide. In the Raman spectra of $CoSb_3$/graphene, two bands at 1350 and 1580 cm^{-1} appear, corresponding to the disordered (D) and graphitic (G) bands of carbon-based materials. Note that compared to graphite oxide, both $CoSb_3$/graphene and graphene exhibit an increased D/G intensity ratio, caused by a reduction of the average size of the sp^2 domains, signifying the reduction of graphite oxide to graphene [58]. It should also be noted that the G peak shows an asymmetric feature. Actually, it is composed of two overlapping peaks, G and D', which are located at 1580 and 1620 cm^{-1}, respectively. The D' peak is a defect peak due to intra-valley scattering [59]. The asymmetric feature of G peak of graphene was also observed in [60, 61].

Fig. 1(d) compares the C1s XPS spectra of graphite oxide and $CoSb_3$/graphene. The XPS spectra can be fitted into four peaks for carbon atoms in four different functional groups: non-oxygenated carbon (C-C or C=C, 284.8 eV), carbon in C-O bonds (286.3 eV), carbonyl carbon (C=O, 287.6 eV) and carboxylate carbon (O-C=O, 289. 0 eV) [53, 58, 62]. Note that the graphite oxide shows a high peak intensity of the non-oxygenated carbon because of the significant oxidation of graphite, in agreement with the XRD results (Fig. 1(b)). Apart from the non-oxygenated carbon, the peak intensity of the other forms of carbon shows a considerable decrease after the solvothermal reaction, indicative of a sufficient reduction of graphite oxide to graphene.

The microstructure of the $CoSb_3$/graphene composite was observed by TEM. Fig. 2(a) shows typical TEM images of the $CoSb_3$/graphene hybrid composed of two overlapped graphene flakes (indicated by arrows A and B) with uniformly loaded $CoSb_3$ nanoparticles. The wavy edges of the flakes reveal that the flakes are rather thin consisting possibly of single or few-layer graphene sheets. Thus, the TEM observation also supports the above assumption that the graphene sheets are separated by the attached $CoSb_3$ particles. It should be noted that nearly all the $CoSb_3$ nanoparticles are attached onto the graphene sheets even though at a low graphene content (5.8 wt %). The $CoSb_3$ nanoparticles can be firmly anchored on the graphene sheets after sonication for morphology observations,

indicating a strong interaction between $CoSb_3$ and graphene, possibly via van der Waals forces [63]. Fig. 2(b) displays typical TEM image of a single flake with folded edges (indicated by the white arrows). The transparent nature also indicates that the graphene flakes are fairly thin constructed likely by single or few-layer graphene sheets.

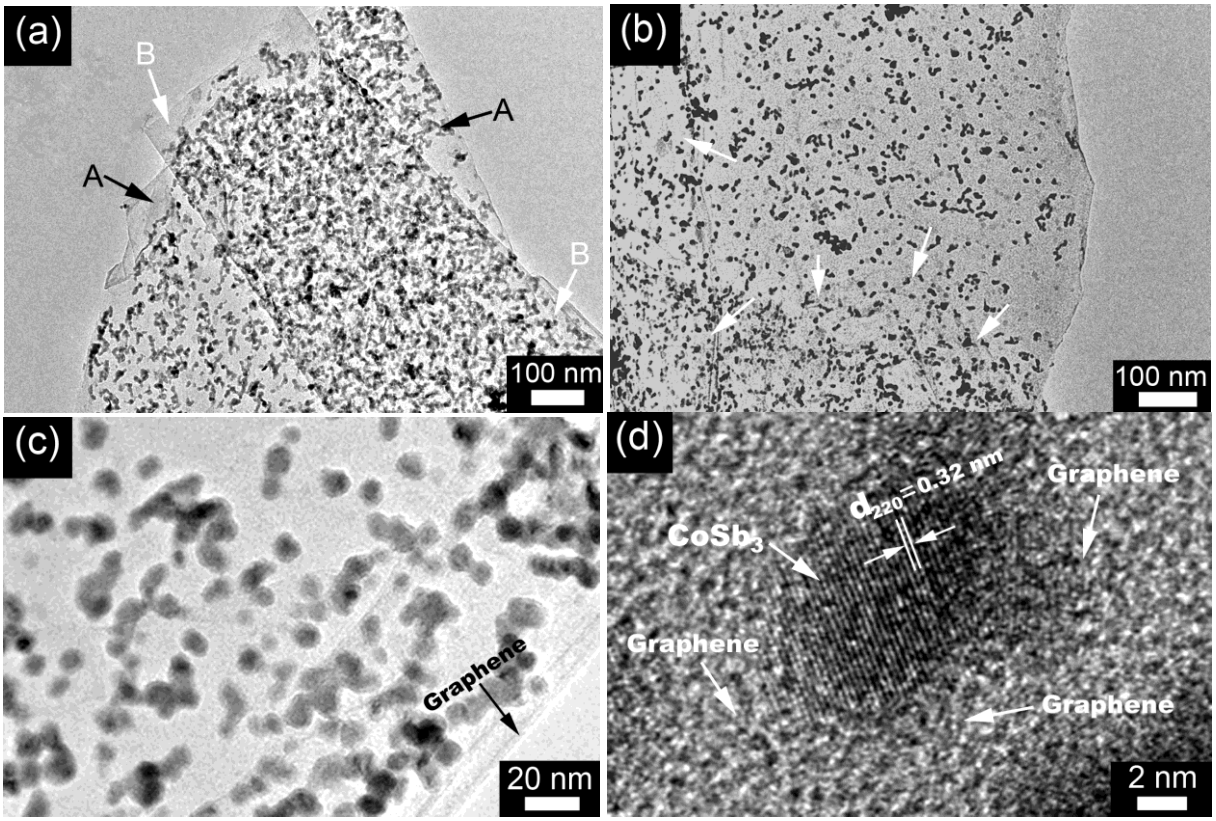

Figure 2. (a, b) low-magnification TEM images, (c) high-magnification TEM images and (d) HRTEM image of $CoSb_3$/graphene.

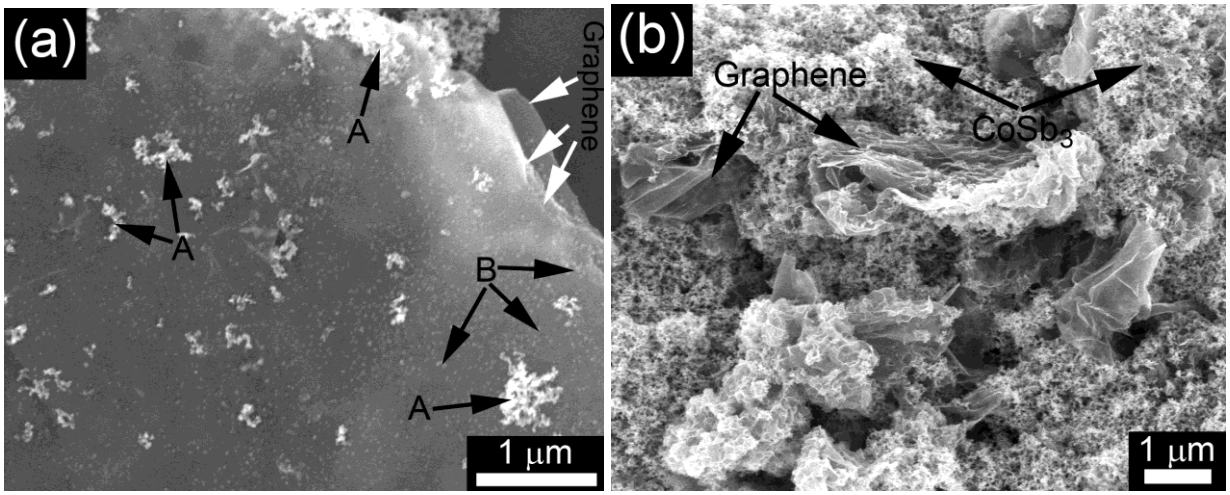

Figure 3. SEM images $CoSb_3$/graphene hybrid prepared by (a) in situ and (b) mechanical mixing route.

Fig. 2(c) shows high-magnification images of the nanocomposite. It is clear that the $CoSb_3$ particles are anchored homogeneously on graphene. The quasi-spheric particles exhibit a rather narrow size distribution with an average size of around 10 nm. Fig. 2(d) shows the lattice resolved HRTEM images of an individual $CoSb_3$ particle on graphene. The fringe spacing is measured to be 0.32 nm, corresponding to the interplanar spacing of (220) plane of $CoSb_3$. From the XRD, Raman, XPS and TEM analyses, it can be concluded that a $CoSb_3$-nanocrystal/graphene hybrid nanostructure has formed during the one-pot in situ solvothermal process.

The $CoSb_3$/graphene nanocomposite was further characterized by SEM. Fig. 3(a) shows a flake of the nanocomposite. From the broken cross section of the flake, it is obvious that a layered structure consisted of alternating $CoSb_3$ nanoparticles and graphene sheets has formed. Through the transparent graphene, it is evident that the $CoSb_3$ nanoparticles (gray particles, denoted by black arrows B) are sandwiched between the graphene sheets. By contrast, the nanoparticles (white particles, denoted by black arrows A) show aggregation without the confinement of the graphene sheets. The SEM images of the mechanically mixed $CoSb_3$ and graphene are also observed as shown in Fig. 3(b). Clearly, both the $CoSb_3$ nanoparticles and the graphene sheets are aggregated when prepared by the ex situ route. The difference in morphology between the in situ prepared and the mechanically mixed samples agrees well with the XRD results, further confirming that the graphene sheets are sufficiently separated by the attached $CoSb_3$ particles. For comparison, the SEM images of bare $CoSb_3$ and bare graphene are also presented in Fig. 4. Note that the $CoSb_3$ nanoparticles tend to aggregate without the support of graphene (Fig. 4(a)). The graphene sheets also aggregate without the attached $CoSb_3$ nanoparticles when comparing A and B parts of bare graphene (Fig. 4(b)).

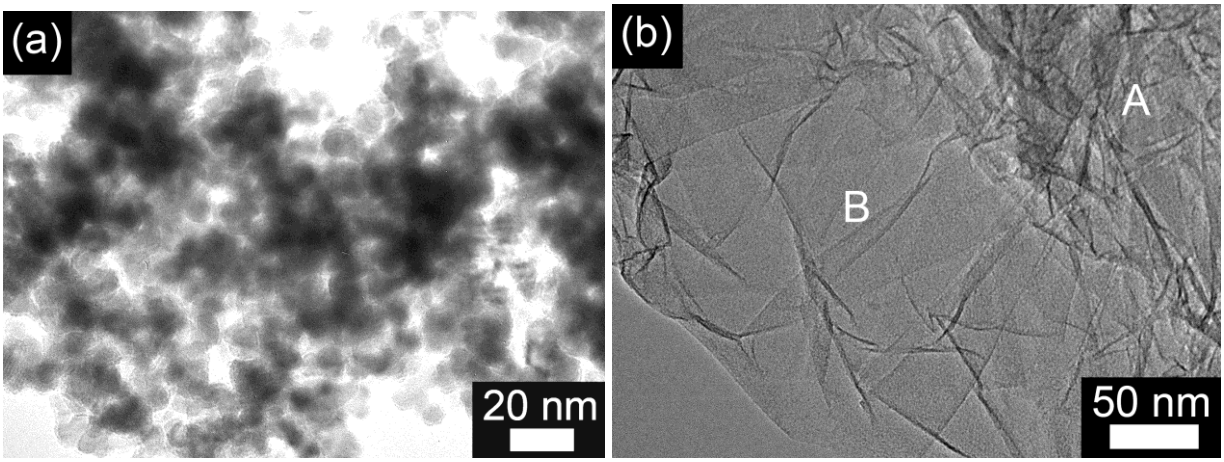

Figure 4. TEM images of (a) bare $CoSb_3$ and (b) graphene.

Based on the above results, the in situ formation mechanism for the $CoSb_3$/graphene nanocomposite is suggested as follows: first, the sufficient exfoliation of the graphite oxide into graphene oxide in ethanol by sonication; second, the uniform dispersion of the precursors on the graphene oxide sheets by their interactions; third, the strong interaction between the product ($CoSb_3$

particles) and the reduced graphene oxide (graphene). The firmly attached $CoSb_3$ nanoparticles, on the other hand, can act as the spacer to prevent the hydrophobic graphene sheets from restacking after reduction.

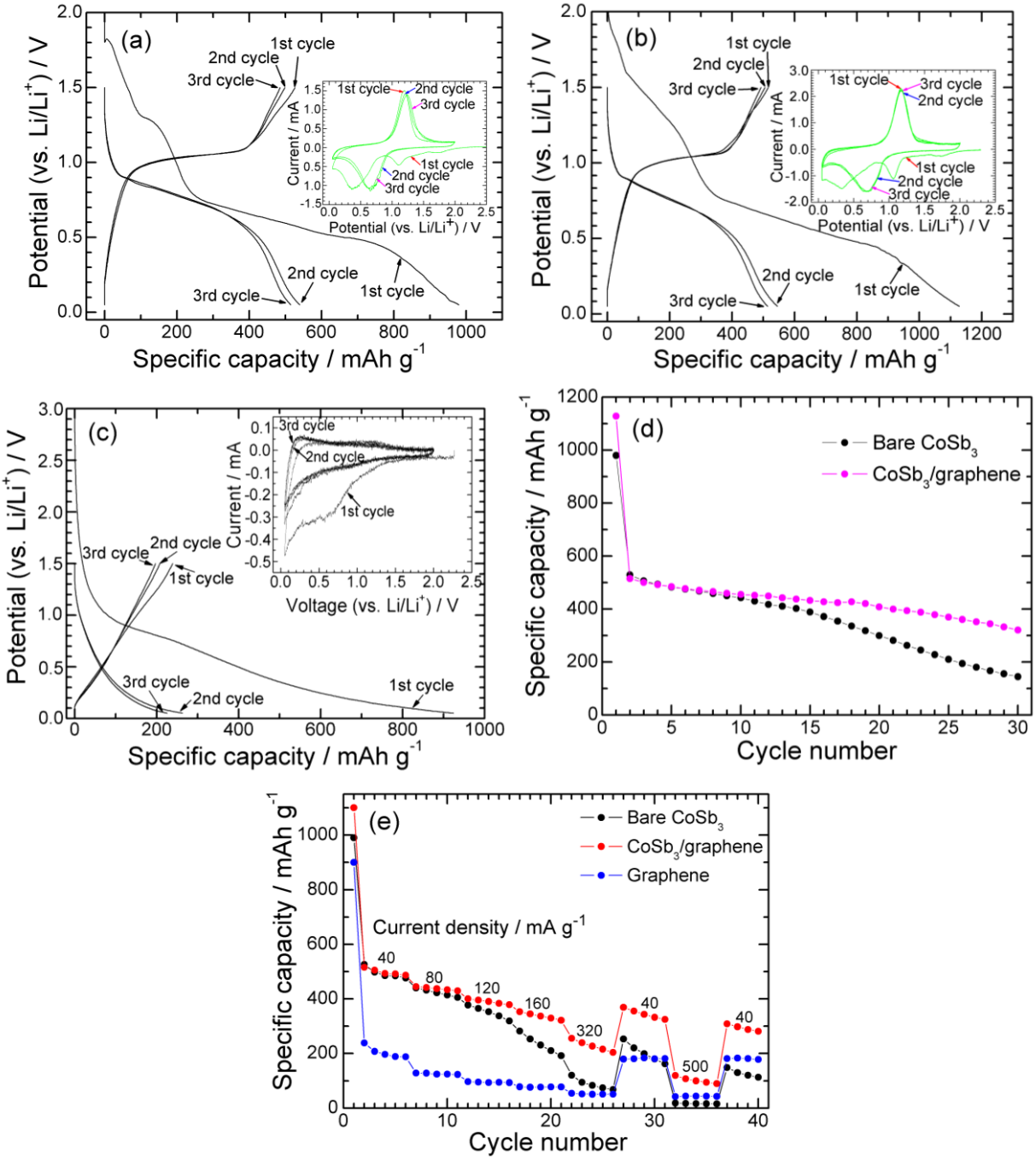

Figure 5. Electrochemical properties of the solvothermal products: charge-discharge curves (40 mA g^{-1}) and CV plots (0.1 mV s^{-1}) of (a) bare $CoSb_3$, (b) $CoSb_3$/graphene, and (c) graphene, (d) comparison of cycling stability between bare $CoSb_3$ and $CoSb_3$/graphene at 40 mA g^{-1}, and (e) comparison of rate capability among bare $CoSb_3$, $CoSb_3$/graphene and graphene.

The electrochemical properties of the $CoSb_3$/graphene nanocomposite and bare $CoSb_3$ were investigated by galvanostatic cycling at 40 mA $g^{-1}$and CV tests at 0.1 mV s^{-1}. The first discharge (Li-absorption) and charge (Li-extraction) capacities of bare $CoSb_3$ are 980 and 526 mAh g^{-1}, respectively (Fig. 5(a)). As seen in Fig. 5(b), $CoSb_3$/graphene gives a higher first discharge capacity (1128 mAh g^{-1}) and slightly lower first charge capacity (516 mAh g^{-1}) compared to bare $CoSb_3$. For both bare $CoSb_3$ and $CoSb_3$/graphene, a quasi-plateau appears in the voltage range of 1−1.5 V, corresponding to the reduction peaks at 1.1 V during the first scan in the CV plots (insets in Fig. 5(a) and (b)). The quasi-plateau is related to the lithiation reaction of Co_3O_4 [64] and Sb_2O_3 [65]. The presence of Co_3O_4 and Sb_2O_3 is one of the sources for the large first irreversible capacities for both the samples since the Li-extraction from lithiated Co_3O_4 occurs mostly over 1.5 V [64] and the reaction of oxygen in Sb_2O_3 with Li is irreversible [65]. The relatively low Li-storage capacity of $CoSb_3$ compared with its theoretical capacity (568 mAh g^{-1}) could also be attributed to the presence of Co_3O_4 and Sb_2O_3. Another origin of the first irreversible capacity is from the decomposition of the electrolyte and the formation of solid electrolyte interface (SEI) layer [8]. After the first cycle, reversible lithiation/delithiation reactions take place evidenced by the almost overlapped charge-discharge curves and CV plots for both the samples, especially for $CoSb_3$/graphene. Fig. 5(c) gives the charge-discharge curves (40 mA g^{-1}) and CV plots (0.1 mV s^{-1}) of bare graphene. Note that the graphene itself exhibits a low reversible capacity and a large first irreversible capacity. This can explain the lower first charge capacity and the higher first irreversible capacity of $CoSb_3$/graphene compared with bare $CoSb_3$.

Fig. 5(d) compares the cycling stability between the nanocomposite and bare $CoSb_3$ at a current density of 40 mA g^{-1}. Obviously, the nanocomposite demonstrates an improved cycling stability compared to bare $CoSb_3$. After 30 cycles, a capacity of 300 mAh g^{-1} can be maintained for $CoSb_3$/graphene, doubling that for bare $CoSb_3$ after the same cycles. The cycling stability of $FeSb_2$ and NiSb was also improved by loading them onto graphene [66]. The enhanced cycling stability can be attributed to the incorporated graphene that not only buffers the large volume changes upon Li-absorption/extraction but also restrains the aggregation of $CoSb_3$ nanoparticles upon prolonged cycling. It should be stressed that the long-term cycling stability of the nanocomposite is not satisfactory yet due to the intrinsically large volume changes of $CoSb_3$.

Fig. 5(e) compares the rate capability among $CoSb_3$/graphene, bare $CoSb_3$ and graphene. Apparently, $CoSb_3$/graphene also shows a better rate capability than bare $CoSb_3$. The improvement in rate capability originates mainly from the following factors: first, the highly conductive graphene offers a two-dimensional (2D) conducting channel for the $CoSb_3$ nanoparticles; second, small-sized, well-dispersed nanoparticles is favorable for rapid Li-ion diffusion; third, the layered structure of the nanocomposite is beneficial for better wetting of the active material by the electrolyte, thus facilitating the faster Li-ion transport across the electrolyte/electrolyte interface.

The electronic conductivities of the samples were measured to understand the different electrochemical behaviors between $CoSb_3$/graphne and bare $CoSb_3$. The room-temperature electronic conductivities for bare $CoSb_3$ and $CoSb_3$/graphene are 3.2×10^4 and 2.1×10^5 Ω^{-1} m^{-1}, respectively, measured by the 4-probe method. The introduction of the 2D conductive graphene can account for the increased electronic conductivity that exerts an important effect on the improved rate capability of the composite.

To further explain the different electrochemical behaviors between bare $CoSb_3$ and $CoSb_3$/graphene, EIS measurements were also carried out. Fig. 6 gives the Nyquist plots of the two samples after 5 and 30 cycles.

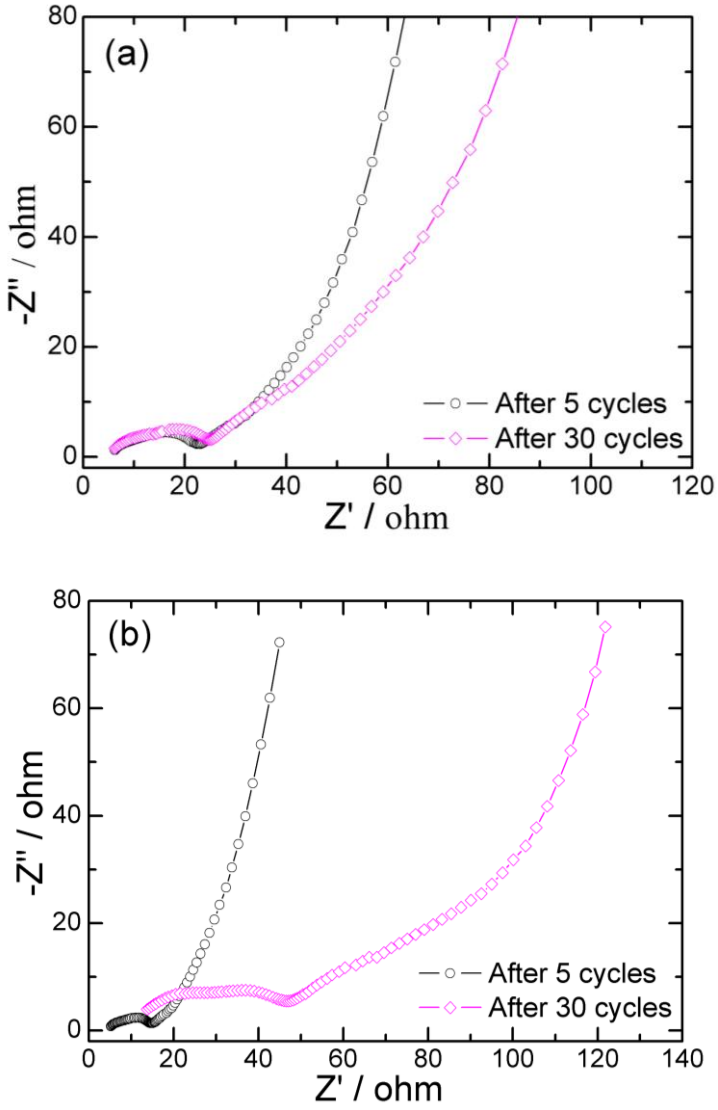

Figure 6. EIS of (a) $CoSb_3$/graphene and (b) bare $CoSb_3$ after 5 and 30 cycles.

Two partially overlapped semicircles in the high-to-medium frequency region and a slopping line in the low frequency region are observed in all the plots. As previously reported [67], the first semicircle is correlated to Li-ions transport resistance through the SEI layer (R_{SEI}), the second one corresponds to the charge transfer resistance (R_{ct}), the slopping line is related to the Li-ion diffusion in the bulk material, and the intercept on the *Z*' axis at high frequency is related to the electrolyte resistance (R_e). For the $CoSb_3$/graphene electrode, R_{SEI} keeps almost unchanged after 5 and 30 cycles (Fig. 6(a)), indicating that the microstructure of the SEI layer is stabilized after the initial cycles. The stabilized SEI layer can block the direct contact of the active material with the electrolyte, preventing

the further reduction decomposition of the electrolyte, which is favorable for the stable and reversible cycling of the electrode. The increase in R_{ct} is also slight for the $CoSb_3$/graphene electrode, indicating that a stable interface between the electrode and the electrolyte has been established. Therefore, constant and fast electrochemical reactions can be kept upon repeated cycling, leading to stable electrochemical cycling and good rate capability. For the bare $CoSb_3$ electrode, in contrast, both R_{SEI} and R_{ct} show an apparent increase during cycling (Fig. 6(b)). An obvious increase in R_e is also observed for the bare $CoSb_3$ electrode during cycling, caused possibly by the exfoliation of the active material into the electrolyte. On the contrary, the $CoSb_3$/graphene electrode exhibits minor change in R_e, implying that the active material shows slight exfoliation from the electrode upon volume changes due to the buffering effect of graphene. This can also explain the better cycling stability of the $CoSb_3$/graphene electrode. As a result, the EIS tests agree well with electrochemical properties.

4. CONCLUSIONS

$CoSb_3$/graphene nanocomposite with a sandwich structure has been synthesized by a simple in situ one-pot solvothermal route. The interaction between the precursors and the interaction between the products are responsible for the formation of this unique hybrid nanostructure. The $CoSb_3$/graphene nanocomposite shows an improved cycling stability and rate capability compared to bare $CoSb_3$. The improvement in cycling stability is attributed to the introduction of the flexible graphene that acts both as a buffer to alleviate the large volume changes and as a separator to hinder the aggregation of the $CoSb_3$ nanoparticles. The introduction of the graphene also offers a 2D conductive network, uniformly disperses the nanoparticles, and increases the wetting of the active material, leading to an enhanced rate capability. The results clearly indicate that the incorporation of graphene can improve the electrochemical performance of the $CoSb_3$ nanoparticles with a potential application as anode for Li-ion batteries.

ACKNOWLEDGEMENTS

This work was supported by Zijin Program of Zhejiang University, China, the Fundamental Research Funds for the Central Universities (No. 2010QNA4003), the Ph.D. Programs Foundation of Ministry of Education of China (No. 20100101120024), the Foundation of Education Office of Zhejiang Province (No. Y201016484), the Qianjiang Talents Project of Science Technology Department of Zhejiang Province (2011R10021), and the National Natural Science Foundation of China (No. 51101139).

References

1. R. Alcántara, F. J. Fernández-Madrigal, P. Lavela, J. L. Tirado, J. C. Jumas, and J. Olivier-Fourcade, *J. Mater. Chem.* 9 (1999) 2517.
2. D. Larcher, L. Y. Beaulieu, O. Mao, A. E. George, and J. R. Dahn, *J. Electrochem. Soc*. 147 (2000) 1703.
3. L. J. Zhang, X. B. Zhao, X. B. Jiang, C. P. Lv, and G. S. Cao, *J. Power Sources* 94 (2001) 92.

4. M. Wachtler, M. Winter, and J. O. Besenhard, *J. Power Sources* 105 (2002**)** 151.
5. J. M. Tarascon, M. Morcrette, L. Dupont, Y. Chabre, C. Payen, D. Larcher, and V. Pralong, *J. Electrochem. Soc.* 150 (2003) A732.
6. C. M. Ionica, P. E. Lippens, J. O. Fourcade, and J. C. Jumas, *J. Power Sources* 146 (2005) 478.
7. I. Sarakonsri, C. S. Johnson, S. A. Hackney, and M. M. Thackeray, *J. Power Sources* 153 (2006) 319.
8. M. Stjerndahl, H. Bryngelsson, T. Gustafsson, J. T. Vaughey, M. M. Thackeray, and K. Edström, *Electrochim. Acta* 52 (2007) 4947.
9. S. Matsuno, M. Nakayama, and M. Wakihara, *J. Electrochem. Soc.* 155 (2008) A61.
10. C. M. Park and H. J. Sohn, *J. Electrochem. Soc.* 157 (2010) A46.
11. N. Dimov, S. Kugino, and M. Yoshio, *J. Power Sources* 136 (2004) 108.
12. J. Xie, X. B. Zhao, G. S. Cao, and M. J. Zhao, *Electrochim. Acta* 50 (2005) 2725.
13. J. X. Zhu, T. Sun, J. S. Chen, W. H. Shi, X. J. Zhang, X. W. Lou, S. Mhaisalkar, H. H. Hng, F. Boey, J. Ma, and Q. Y. Yan, *Chem. Mater.* 22 (2010) 5333.
14. X. B. Zhao, G. S. Cao, C. P. Lv, L. J. Zhang, S. H. Hu, T. J. Zhu, and B. C. Zhou, *J. Alloy Compd.* 315 (2001) 265.
15. L. J. Zhang, X. B. Zhao, and D. G. Xia, *Mater. Lett.* 59 (2005) 3448.
16. K. S. Novoselov, A. K. Geim, S. V. Morozov, D. Jiang, Y. Zhang, S. V. Dubonos, I. V. Grigorieva, and A. A. Firsov, *Science* 306 (2004) 666.
17. S. Park, J. H. An, I. W. Jung, R. D. Piner, S. J. An, X. S. Li, A. Velamakanni, and R. S. Ruoff, *Nano Lett.* 9 (2009) 1593.
18. M. D. Stoller, S. Park, Y. W. Zhu, J. H. An, and R. S. Ruoff, *Nano Lett.* 8 (2008) 3498.
19. C. Lee, X. D. Wei, J. W. Kysar, and J. Hone, *Science* 321 (2008) 385.
20. G. X. Wang, B. Wang, X. L. Wang, J. Park, S. X. Dou, H. Ahn, and K. Kim, *J. Mater. Chem.* 19 (2009) 8378.
21. S. Z. Liang, X. F. Zhu, P. C. Lian, W. S. Yang, and H. H. Wang, *J. Solid State Chem.* 184 (2011) 1400.
22. J. K. Lee, K. B. Smith, C. M. Hayner, and H. H. Kung, *Chem. Commun.* 46 (2010) 2025.
23. S. L. Chou, J. Z. Wang, M. Choucair, H. K. Liu, J. A. Stride, and S. X. Dou, *Electrochem. Commun.* 12 (2010) 303.
24. Z. S. Wu, W. C. Ren, L. Wen, L. B. Gao, J. P. Zhao, Z. P. Chen, G. M. Zhou, F. Li, and H. M. Cheng, *ACS Nano* 4 (2010) 3187.
25. S. Q. Chen and Y. Wang, *J. Mater. Chem.* 20 (2010) 9735.
26. S. B. Yang, X. L. Feng, S. Ivanovici, and K. Müllen, *Angew. Chem. Int. Ed.* 49 (2010) 8408.
27. H. Kim, D. H. Seo, S. W. Kim, J. Kim, and K. Kang, *Carbon* 49 (2011) 326.
28. B. J. Li, H. Q. Cao, J. Shao, G. Q. Li, M. Z. Qu, and G. Yin, *Inorg. Chem.* 50 (2011) 1628.
29. J. X. Zhu, Y. K. Sharma, Z. Y. Zheng X. J. Zhang, M. Srinivasan, S. Mhaisalkar, H. Zhang, H. H. Hng, and Q. Y. Yan, *J. Phys. Chem. C* 115 (2011) 8400.
30. J. X. Zhu, T. Zhu, X. Z. Zhou, Y. Y. Zhang, X. W. Lou, X. D. Chen, H. Zhang, H. H. Hng, and Q. Y. Yan, *Nanoscale* 3 (2011) 1084.
31. G. M. Zhou, D. W. Wang, F. Li, L. L. Zhang, N. Li, Z. S. Wu, L. Wei, G. Q. Lu, and H. M. Cheng, *Chem. Mater.* 22 (2010) 5306.
32. M. Zhang, D. N. Lei, X. M. Yin, L. B. Chen, Q. H. Li, Y. G. Wang, and T. H. Wang, *J. Mater. Chem.* 20 (2010) 5538.
33. P. C. Lian, X. F. Zhu, H. F. Xiang, Z. Li, W. S. Yang, and H. H. Wang, *Electrochim. Acta* 56 (2010) 834.
34. J. Z. Wang, C. Zhong, D. Wexler, N. H. Idris, Z. X. Wang, L. Q. Chen, and H. K. Liu, *Chem. Eur. J.* 17 (2011) 661.
35. B. J. Li, H. Q. Cao, J. Shao, M. Z. Qu, and J. H. Warner, *J. Mater. Chem.* 21 (2011) 5069.

36. L. W. Ji, Z. K. Tan, T. R. Kuykendall, S. Aloni, S. D. Xun, E. Lin, V. Battaglia, and Y. G. Zhang, *Phys. Chem. Chem. Phys.* 13 (2011) 7170.
37. G. Wang, T. Liu, Y. J. Luo, Y. Zhao, Z. Y. Ren, J. B. Bai, and H. Wang, *J. Alloy Compd.* 509 (2011) L216.
38. X. J. Zhu, Y. W. Zhu, S. Murali, M. D. Stoller, and R. S. Ruoff, *ACS Nano* 5 (2011) 3333.
39. B. Wang, X. L. Wu, C. Y. Shu, Y. G. Guo, and C. R. Wang, *J. Mater. Chem.* 20 (2010) 10661.
40. Y. J. Mai, X. L. Wang, J. Y. Xiang, Y. Q. Qiao, D. Zhang, C. D. Gu, and J. P. Tu, *Electrochim. Acta* 56 (2011) 2306.
41. H. L. Wang, L. F. Cui, Y. Yang, H. S. Casalongue, J. T. Robinson, Y. Y. Liang, and H. J. Dai, *J. Am. Chem. Soc.* 132 (2010) 13978.
42. D. H. Wang, D. W. Choi, J. Li, Z. G. Yang, Z. M. Nie, R. Kou, D. H. Hu, C. M. Wang, L. V. Saraf, J. G. Zhang, I. A. Aksay, and J. Liu, *ACS Nano* 3 (2009) 907.
43. Y. C. Qiu, K. Y. Yan, S. H. Yang, L. M. Jin, H. Deng, and W. S. Li, *ACS Nano* 4 (2010) 6515.
44. S. M. Paek, E. Yoo, and I. Honma, *Nano Lett.* 9 (2009) 72.
45. J. Yao, X. P. Shen, B. Wang, H. K. Liu, and G. X. Wang, *Electrochem. Commun.* 11 (2009) 1849.
46. L. S. Zhang, L. Y. Jiang, H. J. Yan, W. D. Wang, W. Wang, W. G. Song, Y. G. Guo, and L. J. Wan, *J. Mater. Chem.* 20 (2010) 5462.
47. D. H. Wang, R. Kou, D. W. Choi, Z. G. Yang, Z. M. Nie, J. Li, L. V. Saraf, D. H. Hu, J. G. Zhang, G. L. Graff, J. Liu, M. A. Pope, and I. A. Aksay, *ACS Nano* 4 (2010) 1587.
48. Y. M. Li, X. J. Lv, J. Lu, and J. H. Li, *J. Phys. Chem. C* 114 (2010) 21770.
49. S. Q. Chen, P. Chen, M. H. Wu, D. Y. Pan, and Y. Wang, *Electrochem. Commun.* 12 (2010) 1302.
50. K. H. Seng, Z. P. Guo, Z. X. Chen, and H. K. Liu, *Adv. Sci. Lett.* 4 (2011) 18.
51. W. S. Hummers and R. E. Offeman, *J. Am. Chem. Soc.* 80 (1958) 1339.
52. J. Xie, X. B. Zhao, G. S. Cao, and S. F. Su, *J. Electrochem. Soc.* 152 (2005) A601.
53. H. J. Shin, K. K. Kim, A. Benayad, S. M. Yoon, H. K. Park, I. S. Jung, M. H. Jin, H. K. Jeong, J. M. Kim, J. Y. Choi, and Y. H. Lee, *Adv. Funct. Mater.* 19 (2009) 1987.
54. J. R. González, R. Alcántara, F. Nacimiento, and J. L. Tirado, *Electrochim. Acta* 56(2011) 9808.
55. Y. C. Si and E. T. Samulski, *Chem. Mater.* 20 (2008) 6972.
56. C. Xu, X. Wang, and J. W. Zhu, *J. Phys. Chem. C* 112 (2008) 19841.
57. D. Li, M. B. Müller, S. Gilje, R. B. Kaner, and G. G. Wallace, *Nat. Nanotechnol.* 3 (2008) 101.
58. S. Stankovich, D. A. Dikin, R. D. Piner, K. A. Kohlhaas, A. Kleinhammes, Y.Y . Jia, Y. Wu, S. T. Nguyen, and R. S. Ruoff, *Carbon* 45 (2007) 1558.
59. A. C. Ferrari, *Solid State Commun.* 143 (2007) 47.
60. G. X. Wang, J. Yang, J. Park, X. L. Gou, B. Wang, H. Liu, and J. Yao, *J. Phys. Chem. C* 112 (2008) 8192.
61. H. L. Wang, J. T. Robinson, X. L. Li, and H. J. Dai, *J. Am. Chem. Soc.* 80 (2009) 9910.
62. S. Stankovich, R. D. Piner, X. Q. Chen, N. Q. Wu, S. T. Nguyen, and R. S. Ruoff, *J. Mater. Chem.* 16 (2006) 155.
63. G. H. Lu, S. Mao, S. Park, R. S. Ruoff, and J. H. Chen, *Nano Res.* 2 (2009) 192.
64. W. Y. Li, L. N. Xu, and J. Chen, *Adv. Funct. Mater.* 15 (2005) 851.
65. H. Li, X. J. Huang, and L. Q. Chen, S*olid State Ionics* 123 (1999) 189.
66. J. Xie, Y. X. Zheng, R. J. Pan, S. Y. Liu, W. T. Song, G. S. Cao, T. J. Zhu, and X. B. Zhao, *Int. J. Electrochem. Sci*. 6 **(**2011**)** 4811.
67. D. Aurbach, *J. Power Sources* 89 (2000) 206.